PDF Turbulence Modeling and DNS

A. T. Hsu

1. Motivations and Objectives

The problem of time discontinuity (or jump condition) in the coalescence/dispersion (C/D) mixing model is addressed in first part (PDF) of this work. A C/D mixing model continuous in time is introduced. With the continuous mixing model, the process of chemical reaction can be fully coupled with mixing. In the case of homogeneous turbulence decay, the new model predicts a pdf very close to a Gaussian distribution, with finite higher moments also close to that of a Gaussian distribution. Results from the continuous mixing model are compared with both experimental data and numerical results from conventional C/D models.

The effect of Coriolis forces on compressible homogeneous turbulence is studied using direct numerical simulation (DNS). The numerical method used in this study is an eigth order compact difference scheme. Contrary to the conclusions reached by previous DNS studies on *incompressible* isotropic turbulence, the present results show that the Coriolis force increases the dissipation rate of turbulent kinetic energy, and that anisotropy develops as the Coriolis force increases. The Taylor-Proudman theory does apply since the derivatives in the direction of the rotation axis vanishes rapidly. A closer analysis reveals that the dissipation rate of the incompressible component of the turbulent kinetic energy indeed decreases with a higher rotation rate, consistent with incompressible flow simulations (Bardina[17]), while the dissipation rate of the Compressible part increases; the net gain is positive. Inertial waves are observed in the simulation results.

2. Work Accomplished

2.1 PDF Turbulence Model for Combustion

In Collaboration with J.Y. Chen

Accurate prediction of turbulent reacting flows requires the solution of an evolution equation for the probability density function (pdf) of the thermo-chemical variables using Monte Carlo simulation. Since the pdf equation, like most equations describing turbulent motion, is not closed, closure models have to be devised. For the pdf of scalars, the terms in the pdf equation that need modeling are molecular mixing and turbulent convection. The present work deals with the modeling of molecular mixing.

Most of the mixing models are based on the coalescence/dispersion (C/D) model by Curl[6] This model is known to have deficiencies, and efforts had been made to correct these deficiencies, for example, Janicka, et al. 1979 and Pope 1982. The most recent efforts have been devoted to the problem of coupling between mixing and chemical reaction. Chen and Kollmann[4] proposed a reaction conditioned model

that allows correct prediction of combustion in the flame-sheet regime. Norris and Pope[10] proposed a new model based on ordered pairing that aimed at the same end.

All the existing models suffer in one respect, namely, they are discontinuous in time: once a pair of particles are chosen to participate in mixing, their properties will jump abruptly regardless of the step size of the time integration. This phenomenon, clearly non-physical, could cause difficulty in coupling the processes of mixing and chemical reaction. In the present work, a new model that is continuous in time is proposed. With this new model, the processes of molecular mixing and chemical reaction can be fully coupled.

In the case of homogeneous turbulence decay of a scalar, one expects a Gaussian distribution for the pdf, and finite values for the higher moments. Pope[11] pointed out the modified Curl model could not produce the correct pdf for this problem, and the higher even moments from that model tend to infinity; he suggested an age biased sampling process to overcome these shortcomings. The present continuous model, as we will show, predicts a pdf distribution very close to Gaussian for homogeneous turbulence decay, and gives finite higher moments with values close to that of a Gaussian distribution.

The continuous mixing model is applied to the study of both non-reacting and reacting flows, and the results are compared with earlier calculations by Hsu[7] as well as with experimental data.

2.1.1 Molecular Mixing Model

The evolution equation of a single point probability density function of scalar random variables $\psi_1, ..., \psi_n$ — representing the species mass fraction and temperature — can be written as

$$\bar{\rho}\partial_t \tilde{P} + \bar{\rho}\tilde{v}_\alpha \partial_\alpha \tilde{P} + \bar{\rho}\sum_{i=1}^{N} \partial_{\psi_i}\{w_i(\psi_1, ..., \psi_N)\tilde{P}\}$$

$$= -\partial_\alpha(\bar{\rho} < v''_\alpha | \phi_k(x) = \psi_k > \tilde{P})$$

$$-\bar{\rho}\sum_{i=1}^{N}\sum_{j=1}^{N} \partial^2_{\psi_i\psi_j}(< \epsilon_{ij} | \phi_k(x) = \psi_k > \tilde{P})$$

where the terms represent the rate of time change, mean convection, chemical reaction, turbulent convection, and molecular mixing, respectively; $\tilde{P}$ is the density-weighted joint pdf:

$$\tilde{P} = \rho P/\bar{\rho},$$

ϵ is the scalar dissipation:

$$\epsilon_{ij} = D\partial_\alpha \phi_i \partial_\alpha \phi_j,$$

(where D is the diffusion coefficient), and $< x|y >$ denotes the mathematical expectation of a random function x conditioned upon y.

The left hand side of the above equation can be evaluated exactly and requires no modeling; the right hand side terms contain the conditional expectation of the

velocity fluctuation and the conditional expectation of the scalar dissipation, which are new unknowns and require modeling. In the present work we concentrate on the modeling of the second term, namely, the conditional expectation of the scalar dissipation, referred to as molecular mixing in the following.

The Modified Curl Model

The simplest and most used mixing model is the modified Curl model, which assumes binary interaction between sample fluid particles. As described by Pope[12] in a Monte Carlo simulation, the continuous pdf is replaced by delta functions

$$P^*(\psi;t) = \frac{1}{N}\sum_{n=1}^{N}\delta(\psi - \phi_n(t)),$$

where each delta function represents one sample fluid particle of an ensemble of N particles. The evolution of P^* entails the movement of the particles in the $\psi-$space, or the evolution of the individual values of ϕ_n's.

With the modified Curl model, the change of ϕ_n due to molecular mixing is achieved by the following binary interaction process: divide the flow domain into small cells, each containing N sample particles. Given a small time interval δt and a turbulent time scale τ, select randomly N_{mx} pairs of particles,

$$N_{mx} = 0.5\frac{\delta t}{C\tau}N,$$

$(C = 6.0)$ and let a pair, say, m and n, mix as follows

$$\phi_n(t+\delta t) = A\phi_m(t) + (1-A)\phi_n(t) \tag{1}$$

$$\phi_m(t+\delta t) = A\phi_n(t) + (1-A)\phi_m(t) \tag{2}$$

where $A = 0.5\xi$, with ξ a random variable uniformly distributed on the interval [0,1]. The remaining $N - 2N_{mx}$ particles remain unchanged:

$$\phi_n(t+\delta t) = \phi_n(t)$$

This model does not represent the true physical process since the properties of the sample particles change discontinuously regardless the size of the time interval δt. This deficiency can be best illustrated by rearranging eq. (1) and dividing it by δt

$$\frac{(\phi_n(t+\delta t) - \phi_n(t))}{\delta t} = \frac{A}{\delta t}(\phi_m(t) - \phi_n(t)) \tag{3}$$

The derivative $\frac{d\phi_n}{dt}$ does not exist because as δt goes to zero the right hand side of the equation becomes infinite since both A and the difference between $\phi_m(t)$ and $\phi_n(t)$ are finite. This means that there is a sudden jump in the value of the scalar quantities, which is typical of a Poisson process, but is non-physical in the present case since the flow properties of turbulence are continuous.

Continuous Mixing Model

One can see from the previous section that the modified Curl model relies on the parameter N_{mx} to control the extent of mixing. On the individual particle level, it assumes complete mixing once the particle is selected as one of the mixing pair, without considering the size of δt.

In order to achieve continuous mixing, we propose the following model: during a time interval δt, we assume that all the particles within a cell participate in mixing. The extent of the mixing is controlled at the individual particle level. That is to say, the N particles within a given cell are randomly grouped into $N/2$ pairs; the properties of all the particles change according to eqs. (1) and (2) The extent of mixing now has to be controlled at the individual particle level through the parameter A, which is redefined as

$$A = C' \xi \frac{\delta t}{\tau}$$

where $C' = 2.0$. With this new definition, eq. (3) can be written, in the limit $\delta t \to 0$,

$$\frac{d\phi_n}{dt} = C' \frac{\xi}{\tau} (\phi_m(t) - \phi_n(t)).$$

The above equation states that the change of ϕ_n due to mixing is proportional to the difference between ϕ_m and ϕ_n, and inversely proportional to the turbulence time scale τ.

The Coupling of Mixing and Reaction

The processes of mixing and chemical reaction are essentially decoupled when one uses the discontinuous C/D models. In contrast, with the above continuous model, coupling becomes natural since, for a given particle, mixing and chemical reaction can be described with a single equation:

$$\frac{d\phi_n}{dt} = C' \frac{\xi}{\tau} (\phi_m(t) - \phi_n(t)) + w_n,$$

where w_n is the chemical source term.

Since the continuous mixing model allows full coupling of the reaction and mixing processes, the C/D model with reaction zone conditioning by Chen and Kollmann[4] can be easily implemented in the present model to simulate the fast reaction in the flame sheet regime. Here a modified finite difference version of eq. 12 has to be used since w_n is infinity in case of fast reaction.

2.1.2 Results and Discussions

The continuous mixing model described in the previous section has been validated using both non-reacting and reacting flow test cases. The results and their comparisons with earlier calculations (Hsu[7]) using the modified Curl model as well as with experimental data are presented in this section.

Homogeneous Turbulence Decay of a Scalar

The case of decaying fluctuation of a passive scalar in homogeneous turbulence is used to test the continuous mixing model. The initial condition is

$$P^*(\psi;t) = \frac{1}{N}\left[\sum_{n=1}^{N/2}\delta(\psi-1) + \sum_{n=N/2+1}^{N}\delta(\psi+1)\right],$$

that is, in the Monte Carlo simulation, half of the particles are ascribed the value 1, and the other half -1.

The pdf distribution of the normalized variable $(\psi - < \phi >)/\sigma$, where $< \phi >$ is the mean and σ is the standard deviation, in the homogeneous turbulence decay problem converges to a single curve after certain time, and the correct distribution should be Gaussian. Fig. 1 and 2 are the pdf distributions from the modified Curl model and the present model, both compared to a normal distribution. One can see that the pdf from the modified Curl model deviates considerable from Gaussian, while the result from the present model is fairly close to a Gaussian distribution.

The evolution history of the rms and fourth and sixth moments of the scalar fluctuation are calculated using both the modified Curl model and the present continuous model. Fig. 3 shows the results from the modified Curl model. One can see that although the rms from that model behaves well, the fourth and sixth moments grow quickly out of bound, oscillating at a level several order of magnitudes higher than the value of Gaussian distribution. These results are similar to what Pope[11] had observed. Fig. 4 shows the results for the same set of quantities from the present model. The rms behaves similar to that from the modified Curl model. The fourth and sixth moments, on the other hand, are quite different from those of the previous model; they rise smoothly to the value predicted by Gaussian distribution. Although the values do not seem to converge, they remain finite, and are of the same order of magnitude as that of the Gaussian distribution.

The above results clearly demonstrated the advantage of the present model over that of the modified Curl model. Pope[11] had devised an age biased scheme that achieved the same end, which required an additional variable, namely the age of the particles, and two extra adjustable parameters. In contrast, the present model needs no extra work or parameters.

Heated Turbulent Jet

Extensive experimental results for a heated turbulent plane jet have been reported by many authors (Bashir, et al.[2], Browne et al.[3], Uberoi and Singh[13], Jenkins[9], Antonia, et al.[1]). The turbulent jet has a slightly higher temperature than the ambient. Measurements of both the the mean temperature and the rms of temperature fluctuations were given. We compared the solutions for the heated turbulent jet from the new model with experimental data as well as with previous solutions (Hsu[7]) obtained using the modified Curl model.

In the present study, a combined CFD—Monte Carlo algorithm is used. The mean flow field is obtained by solving the Navier-Stokes equation and a two-equation

turbulence model using a finite difference scheme. The temperature is treated as a conserved scalar and simulated by the pdf equation.

Fig. 5 shows the comparisons of the the mean temperature distribution from the pdf Monte Carlo simulations and experimental data from various authors. The figure shows that both mixing models predict the mean temperature distribution accurately.

The results for standard variation, or rms, of the temperature distribution are given in Fig. 6. Although the two solutions do not show significant difference, the new model seems to agree slightly better with the experimental data. The skewness and the flatness, i.e., the third and fourth moments of the temperature fluctuation, are given in Figs. 7 and 8; the comparisons show that in the present case of a turbulent jet the statistical behavior of the new model is similar to that of the modified Curl model.

Hydrogen-Fluorine Diffusion Flame

The continuous model has been applied to the H_2—F_2 diffusion flame studied earlier by Hsu[7]. The flow conditions are set according to an experiment performed by Hermanson and Dimotakis[6]. The flame consists two streams. The upper stream contains 96% of N_2 and 4% of F_2, the flow velocity is $U_1 = 22\,m/s$; the lower stream contains 96% of N_2 and 4% of H_2, with velocity $U_2 = 8.8\,m/s$. The estimated Damköhler number ranged from 25 to 130 (Hermanson and Dimotakis[6]), and a fast chemistry model is deemed appropriate in the calculation. Again a modified version of eq. 12 is used to accommodate the fast chemistry.

Fig. 9 shows the temperature rise due to combustion. In the figure, δ_T is the shear layer thickness determined by 1% of the temperature rise, ΔT is the actual temperature rise due to combustion, (the two streams have the same temperatures initially,) and ΔT_{adf} is the adiabatic flame temperature assuming complete reaction. Details on the flow conditions can be found in Hermanson and Dimotakis[6]. The agreement between numerical predictions and experimental data is fairly good, and a comparison of the results from the continuous model and that from the modified Curl model shows that both performed well for this case.

Combination with Reaction Zone Conditioning

Chen and Kollmann[4] developed a mixing model based on reaction zone conditioning, aimed at the coupling of reaction and mixing. We have shown in Section 2.3 that with the present model, the processes of reaction and mixing can be fully coupled; therefore it is only natural to apply the reaction zone conditioning suggested by Chen and Kollmann here.

The H_2—F_2 diffusion flame problem is reformulated such that the chemical reaction is confined to a very narrow zone near stoichiometry. By applying reaction zone conditioning to the continuous mixing model, we were able to produce a scatter plot of the temperature vs. mixture fraction in which all the points reached the equilibrium temperature. This result is shown in Fig. 10. The mixture fraction here is defined as the molar concentration of fuel divided by the total molar concentration, and stoichiometry is located at $f = 0.5$.

2.1.3 Conclusions

A turbulence mixing model that is continuous in time has been introduced. The deficiency of non-physical jump condition in the mixing process is removed in the new model. It has been shown that the new model is superior to the existing modified Curl model (Janicka, et al.[8]) in that it can predict a Gaussian distribution and finite higher moments in the case of homogeneous turbulence decay; it has accomplished what the age biased sampling scheme (Pope[11]) is designed for, without the extra parameters required by that scheme. The numerical results from the present model compare well with experimental data.

2.2 DNS of Homogeneous Compressible Turbulence in a Rotating frame

Rotation is an important factor in many flow phenomena in nature and in engineering. Problems that are strongly affected by rotation include flows in turbomachinery, large scale motions in the atmosphere and oceans, and galactic motions. Turbulence is important in all the above examples. In order to model turbulence in a rotating frame, we need a better understanding on the effects of rotation on turbulence.

Several experiments had been carried out by various researchers[14–16]. However, the conclusions are inconsistent. Some results show that rotation increases the turbulence dissipation rate, others suggest the opposite.

Numerical studies of turbulence in a rotating frame are few. In fact the only two are incompressible flow studies, by Bardina, et al.[17] and by Speziale et al.[18], using the same computer program. Studies other than the present one dealing with compressible flows in a rotating frame are not known to the authors.

Bardina et al.[17] performed both large eddy and full simulations of incompressible isotropic turbulence. Their results show that, in the case of *incompressible* turbulence, the dissipation rate decreases with increasing rotation rate, and that anisotropy does not develop as a result of the Coriolis force. Speziale et al. confirmed these results using a smaller Rossby number, i.e. a faster rotation.

In general, compressible turbulence in a rotating frame is not homogenous or isotropic because of the existence of centrifugal force and density fluctuations. However, when the rotation rate is low, or when the solution domain is very close to the rotation axis, the centrifugal force can be neglected and the flow is approximately homogeneous. In the present study, our goal is to identify the effects of the Coriolis force, as opposed to the effects of the centrifugal force or the combined effects of the centrifugal and Coriolis forces. Therefore, the centrifugal force is dropped from the governing equations, regardless of whether or not it is negligible. A future study will concentrate on the non-homogenous effects of the centrifugal force and the combined effects of the two forces.

The numerical results presented in the following show that although the Coriolis force does not appear explicitly in the turbulence kinetic energy equation, its effect can be significant. Anisotropy does develop as a result of the Coriolis force. The dissipation rate of the compressible and incompressible modes of the turbulent kinetic energy behave differently under Coriolis forces, and the combined effect is a

increased dissipation rate.

2.2.1 Method

The governing equations for compressible flows in a rotating frame are

$$\rho_{,t} + (\rho u_j)_{,j} = 0$$
$$(\rho u_i)_{,t} + (\rho u_j u_i)_{,j} = -p_{,i} + \tau_{ij,j} - \rho\epsilon_{ijk}\epsilon_{klm}\Omega_j\Omega_l x_m - 2\rho\epsilon_{ijk}\Omega_j u_k$$
$$(\rho e)_{,t} + (\rho u_j e)_{,j} = -pu_{j,j} + u_{i,j}\tau_{ij} - (kT_{,j})_{,j}$$
$$p = \rho RT$$

The last two terms in the second equation represent, respectively, the effects of centrifugal force and the Coriolis force. The centrifugal force is a nonuniform body force which would induce nonuniform pressure and density distributions; its effect on turbulence is to destroy homogeneity. The Coriolis force, on the other hand, is a uniform body force, provided that the velocity field is uniform. In the case of incompressible flows, the centrifugal force can be included into a modified pressure term and thus does not appear explicitly; however, this can not be done in the case of compressible flows.

In order to identify the homogeneous effect of the Coriolis force alone, and to compare results with incompressible flow simulations, we simply take away the centrifugal force in our study. This, of course, greatly simplifies the problem: With a homogeneous initial condition, the flow field remains homogeneous under the Coriolis force. The simplified problem is a hypothetical one and can not normally be found in nature except in very restricted situations such as the ones mentioned in the introduction.

The governing equations are solved using a compact difference scheme. Lele[19] has shown that such schemes have spectral accuracy and are well suited for DNS. The spatial derivatives are approximated by 8th order finite differences, and the time integration is performed using a three-stage Runge-Kutta time marching scheme.

The initial condition for the rotating flow simulation is obtained from a simulation of isotropic decaying turbulence. The initial condition for the decaying turbulence is generated using a given 3D spectrum of the form

$$k^4 exp\left[-2\left(\frac{k}{k_0}\right)^2\right].$$

After the decaying turbulence shows the correct skewness, the Coriolis force is imposed onto the flow field.

2.2.2 Results and Discussion

As a primary study, three cases have been calculated, with rotation in the z-direction: The nondimensional rotation rates are Ω = 0, 40, 80, which correspond to turbulent Rossby numbers of ∞, 0.0075, and 0.00375. These Rossby numbers are much smaller than those considered in References 17 and 18.

Figures 11 and 12 show the development of a 1D two-point correlation and a 1D spectrum in the turbulent flow field, where square symbols are initial conditions and lines represent later times. Figure 13 shows a comparison of the energy spectrum obtained using two different grids, one double the size of the other. The agreement affirms sufficient resolution.

Figures 14-19 show the time history of various statistics of the three cases, where time is nondimensionalized using the initial eddy turn over time.

Figure 14 is the ratio of the turbulent kinetic energy, where q_0^2 is the initial turbulent kinetic energy and q^2 the value at later times. It is immediately clear that the Coriolis force causes a faster decay of the turbulence, a conclusion that is contrary to what was observed in the incompressible flow simulations by previous researchers[17,18]. Nevertheless, as we shall see in the following, the present results are in fact consistent with those of Refs 4 and 5.

To prove that the present results are consistent with the previous incompressible simulations, we look at the ratio of the means of the divergence squared and vorticity squared, which are proportional to, respectively, the compressible and incompressible turbulent kinetic energy. Figures 15 and 16 show that while the dissipation rate of the compressible part of the turbulent kinetic energy increases with larger Coriolis forces, the dissipation rate of the *incompressible* part decreases. The combined effect, as we have seen from Figure 14, is an increase in the total dissipation rate. Since the simulations of References 4 and 5 are for incompressible flows, it is not surprising that only a decrease in dissipation rate was observed.

In both References 17 and 18, no anisotropy was observed. Bardina et al.[17] speculated that a reorganization to two-dimensional flows could occur at higher rotation rates, while Speziale et al. suggested that Taylor-Proudman reorganization would not occur in a rapidly rotating isotropic turbulence. The present results show definite signs of anisotropy as soon as the Coriolis force is turned on. The anisotropy can be clearly observed from the time history of the normal components of the Reynolds stress, given in Figures 17, 18, and 19 for the three rotation rates. With the Coriolis force, the x- and y-components of the normal Reynolds stress decrease much faster than the z-component. In fact, it seems that the increased dissipation is primarily in the x- and y-directions, and the z-component of the turbulent kinetic energy is not affected much.

The Taylor-Proudman theory stipulates that under strong rotation, with the rotation axis parallel to, say, the z axis, then for any flow variable u, we have $(\partial u/\partial z) = 0$. Figures 20 and 21 are the contours of the x-component of velocity plotted on three planes. Without the Coriolis force (Figure 20), the flow structure remains isotropic. With the Coriolis force, columns soon appear in the flow field, suggesting that a Taylor-Proudman reorganization has occurred. Using larger Rossby numbers such as those used in References 17 and 18, the results show no appreciable anisotropy, hence there appears to be no contradiction.

Finally, inertial waves can be observed from the time history of various statistics presented in Figures 14-19. The frequency is approximately Ω/π, the theoretical intrinsic frequency for rotating flows.

3. Future Work

3.1 PDF

The pdf model is being implemented into an existing compressible flow solver: the RPLUS2D code. Work on implementing pdf to RPLUS3D will follow.

3.2 DNS

To understand the effect of compressibility, incompressible homogeneous turbulence in a rotating frame will be studied.

4. References

1 Antonia, R.A., Browne, L.W.B., Chambers, A.J., and Rajagopalan, S., "Budget of the Temperature Variance in a Turbulent Plane Jet." Int. J. Heat Mass Transfer,**26-1**, 41-48, (1983).

2 Ashir, J. and Uberoi, M.S., "Experiments on Turbulent Structure and Heat Transfer in a Two Dimensional Jet." Physics of FLuids, **18-4**, 405-410, (1975).

3 Browne, L.W.B., Antonia, R.A., and Chembers, A.J., "The Interaction Region of a Turbulent Plane Jet." J. Fluid Mech., **149,** 355-373, (1984).

4 Chen, J.-Y. and Kollmann, W., "Mixing Models for Turbulent Flows with Exothermic Reactions." Turbulent Shear Flows, Springer-Verlag, **7**, 277, (1991).

5 Curl, R.L., "Dispersed Phase Mixing, I, Theory and Effects of Simple Reactors." A.I.Ch.E.J. **9**, 175, (1963).

6 Hermanson, J.C. and Dimotakis, P.E., "Effects of Heat Release in a Turbulent, Reacting Shear Layer." J. Fluid Mech. **199**, 333-375, (1989).

7 Hsu, A.T., "The Study of Hydrogen Diffusion Flames Using PDF Turbulence Models." AIAA Paper 91-1780, (1991).

8 Janicka, J., Kolbe, W., and Kollmann, W., "Closure of the Transport Equation for the Probability Density Function Scalar Field." J Non-Equilib. Thermodyn. **4**, 47, (1979).

9 Jenkins, P.E. and Goldschmidt, V.W., "Mean Temperature and Velocity in a Plane Turbulent Jet," ASME J. Fluids Eng., **95**, 581-584, (1973).

10 Norris, A.T. and Pope, S.B., "Turbulent Mixing Model Based on Ordered Pairing." Combust. and Flame, **83,** 27-42, (1991).

11 Pope, S.B., "An Improved Turbulence Mixing Model." Combust. Sci. Tech., **28**, 131, (1982).

12 Pope, S.B., "PDF Methods for Turbulent Reactive Flows." Prg. Energy Combust. Sci., **11**, 119-192, (1985).

13 Uberoi, M.S. and Singh, P.I., "Turbulent Mixing in a Two-Dimensional jet," Physics of Fluids, **18-7,** 764-769, (1975).

14 Traugott, S.C., "Influence of Solid-body Rotation on Screen-produced Turbulence." NACA TN 4135, (1958).

15 Ibbetson, A. and Tritton, D.J., " Experiments on Turbulence in a Rotating Fluid." J. Fluid Mech., **56**, 639-672, (1975).

[16] Wigeland, R.A. and Nagib, H.M. "Grid-generated Turbulence With and Without Rotation About the Streamwise Direction." IIT Fluids and Heat Transfer Rep. R78-1, Illinois Inst. of Tech., Chicago, Illinois, (1978).

[17] Bardina, J., Ferziger, J.H. and Rogallo, R.S. "Effect of Rotation on Isotropic Turbulence: Computation and Modeling," J. Fluid Mech., **154**, 321-336, (1985).

[18] Speziale, C.G., Mansour, N.N. and Rogallo, R.S., "The Decay of Isotropic Turbulence in a Rapidly Rotating Frame," Center for Turbulence Research, Proceedings of the Summer Program, (1987).

[19] Lele, S.K., "Compact Finite Difference Schemes with Spectral Like Resolution." Submitted to J. Comp. Physics.

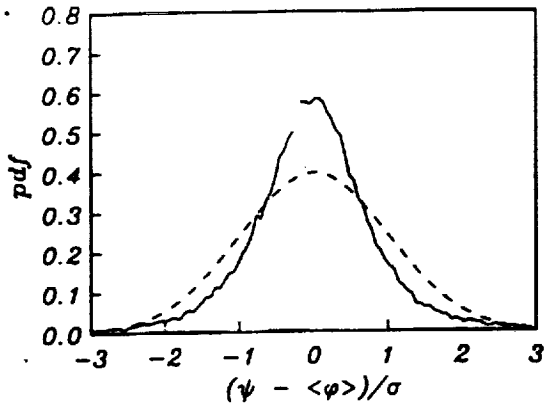

Figure 1. Asymptotic pdf distribution for a scalar in homogeneous turbulence. — modified Curl model; - - - Gaussian.

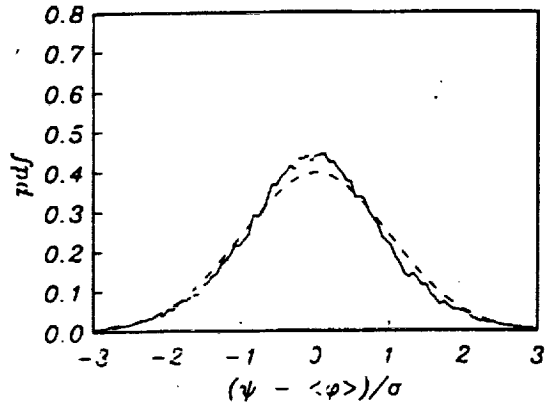

Figure 2. Asymptotic pdf distribution for a scalar in homogeneous turbulence. — present model; - - - Gaussian.

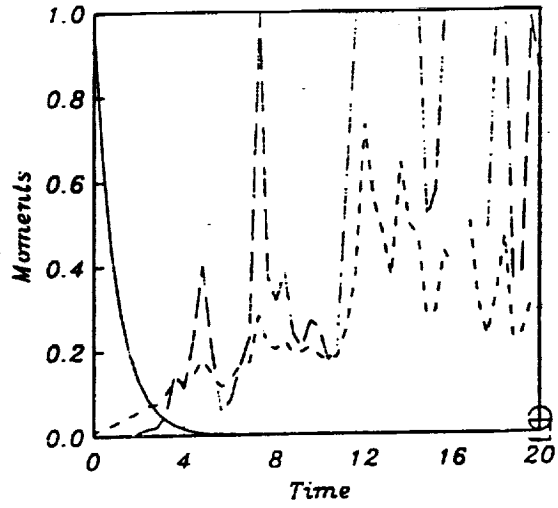

Figure 3. Evolution of moments from the modified Curl model. — standard deviation, - - - 0.01 × fourth central moment, – – 0.0001 × sixth central moment, ∘ 0.01 × fourth moment for Gaussian distribution, □ 0.0001 × sixth moment for Gaussian distribution.

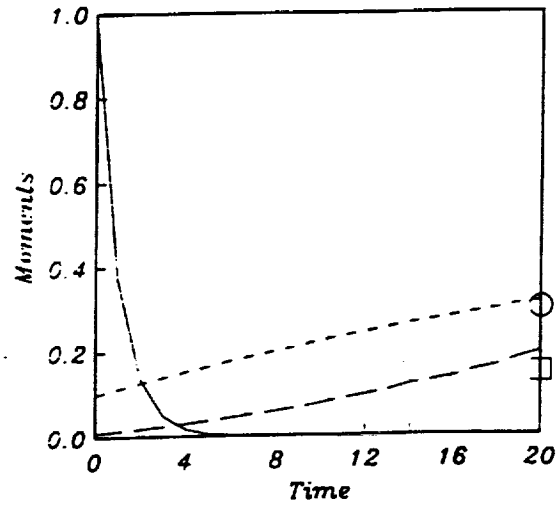

Figure 4. Evolution of moments from the present model. — standard deviation, - - - 0.1 × fourth central moment, – – 0.01 × sixth central moment, ∘ 0.1 × fourth moment for Gaussian distribution, □ 0.01 × sixth moment for Gaussian distribution.

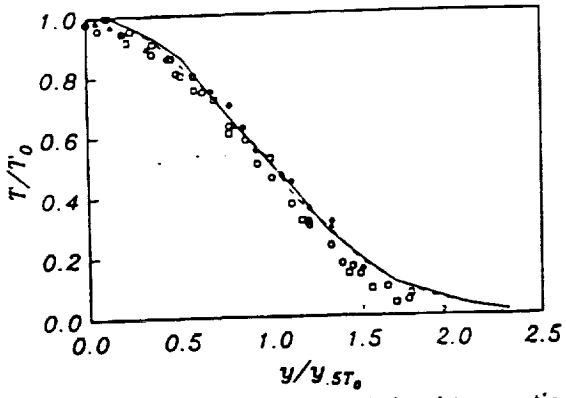

Figure 5. Mean temperature in heated plane jet. — continuous mixing model, - - - modified Curl model, Δ Browne et al. (1984), □ Bashir and Uberoi (1975), ◇ Uberoi and Singh (1975), ○ Jenkins and Goldschmidt (1973).

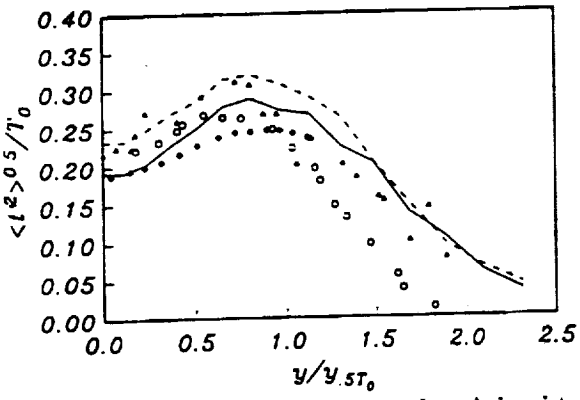

Figure 6. RMS of temperature variance in heated plane jet. — continuous mixing model, - - - modified Curl model, ◇ Antonia et al. (1983), ○ Bashir and Uberoi (1975), Δ Uberoi and Singh (1975).

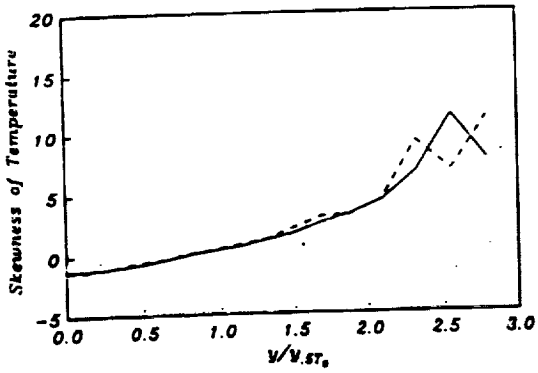

Figure 7. Skewness of temperature variance in heated plane jet. — continuous mixing model, - - - modified Curl model.

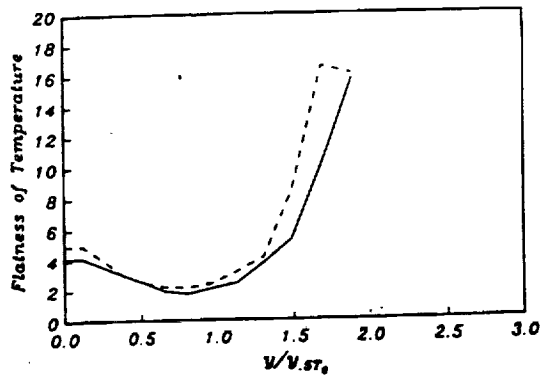

Figure 8. Flatness of temperature variance in heated plane jet. — continuous mixing model, - - - modified Curl model.

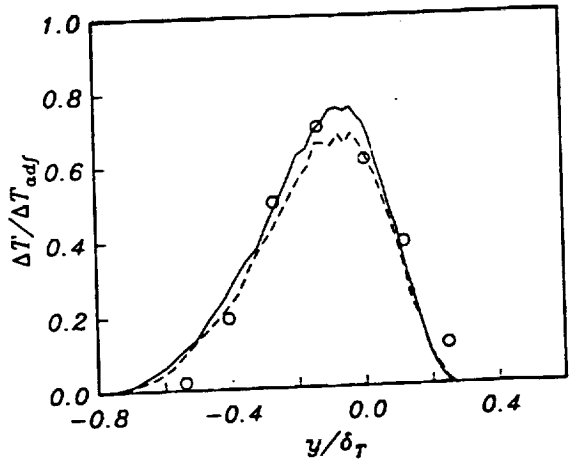

Figure 9. Temperature rise in an H_2–F_2 diffusion flame. — continuous mixing model, - - - modified Curl model, ○ Hermanson and Dimotakis (1989).

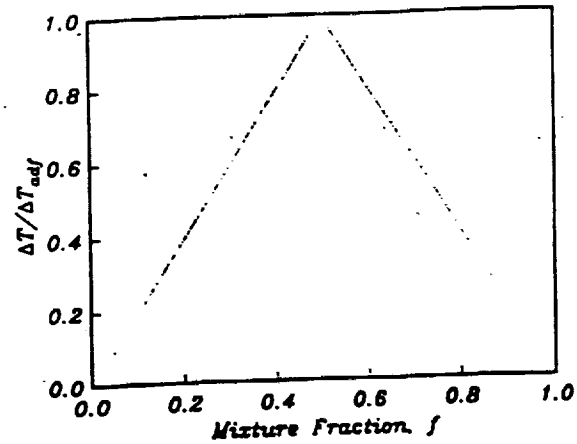

Figure 10. Joint pdf between temperature and mixture fraction on the centerline of the H_2–F_2 diffusion flame; reaction is restricted to a narrow zone at stoichiometry; results are obtained by applying reaction zone conditioning (Chen and Kollmann, 1990) to the continuous mixing model.

Fig. 11 *1D Corelation*

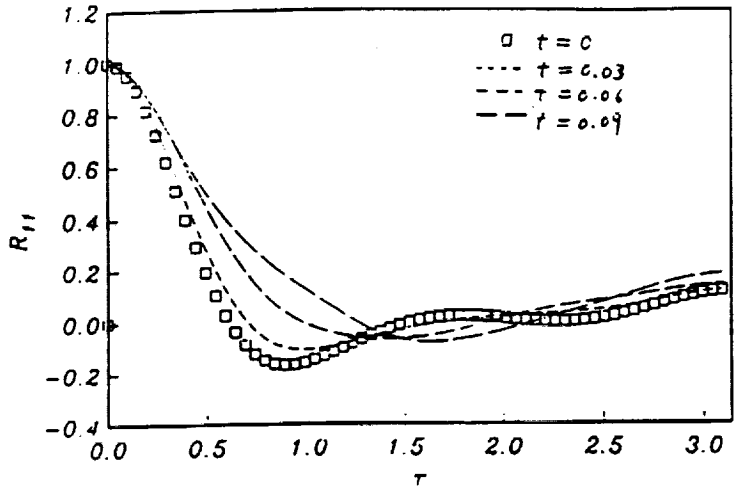

Fig. 12 *1D Spectrum*

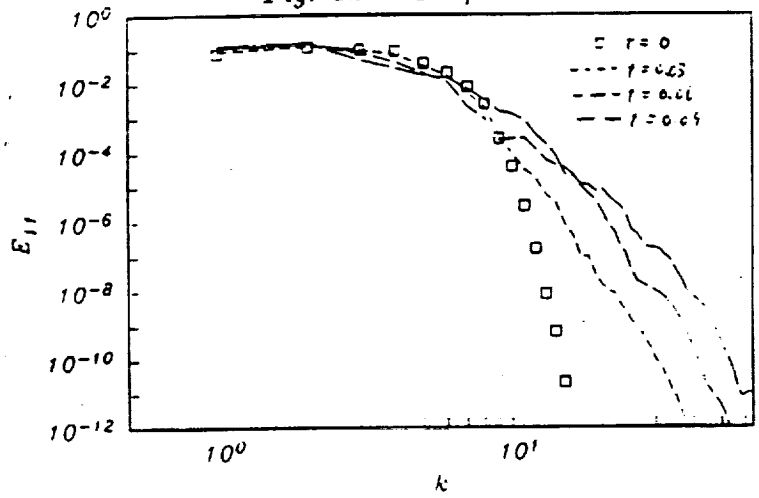

Fig. 13 *Energy Spectrum*

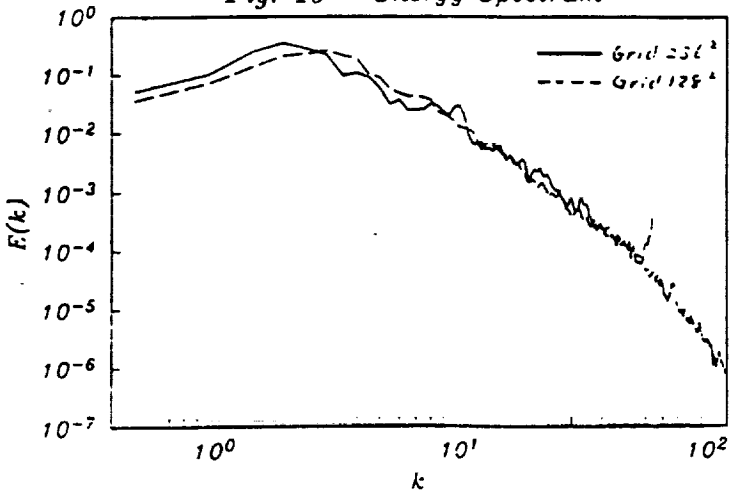

Fig.14 Turbulent kinetic energy

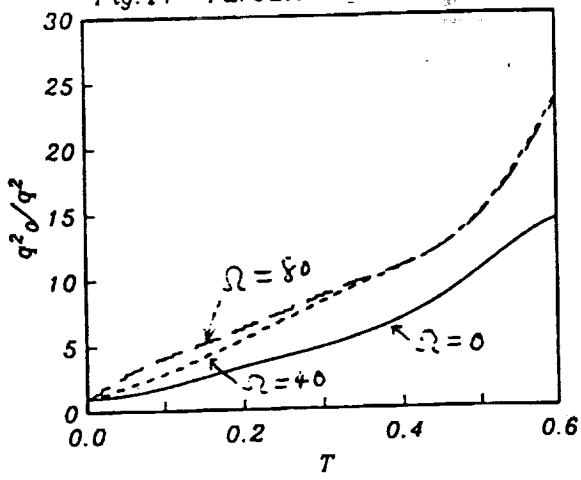

Fig.15 Compresseble energey ratio.

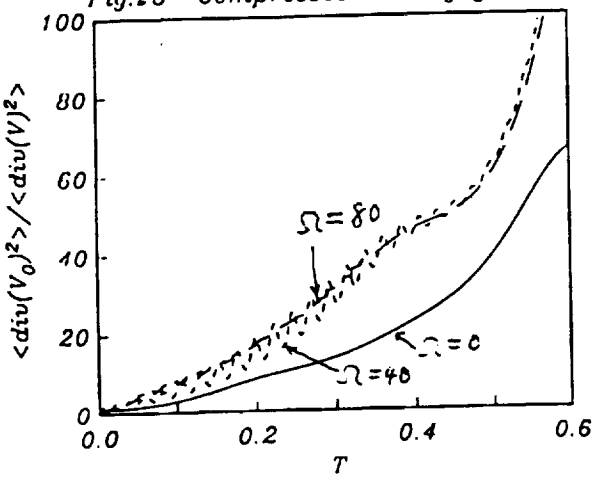

Fig.16 Incompresseble energey ratio.

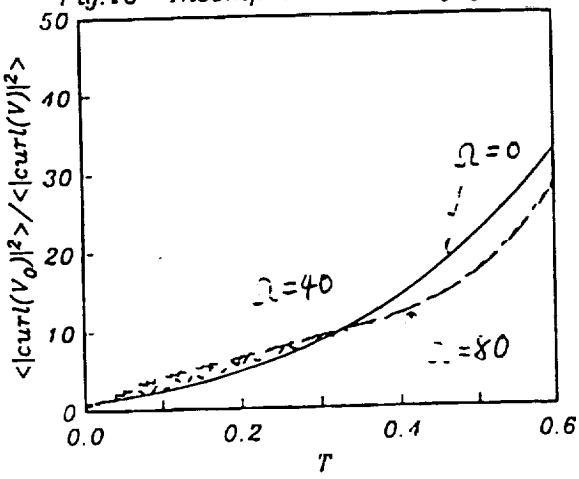

Fig.17 Reynolds stresses, Ω =0., Re=20

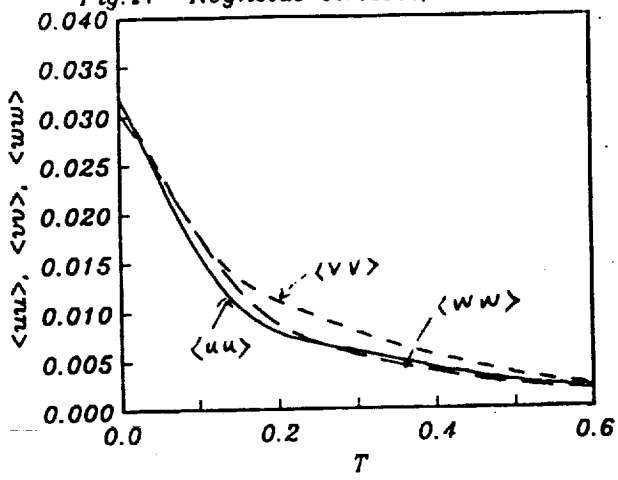

Fig.18 Reynolds stresses, Ω =40., Re=20

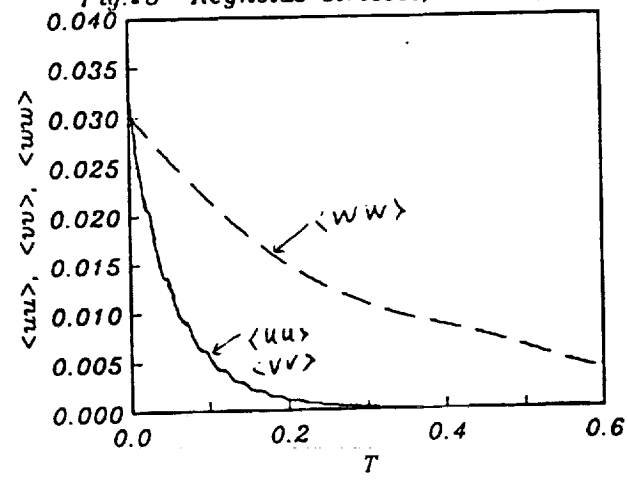

Fig.19 Reynolds stresses, Ω =80., Re=20

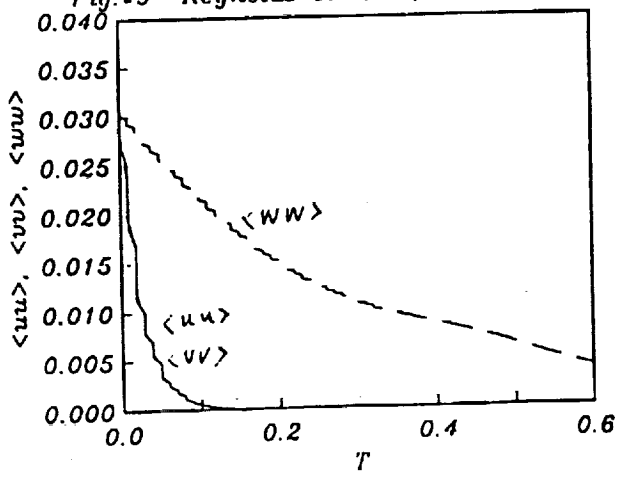

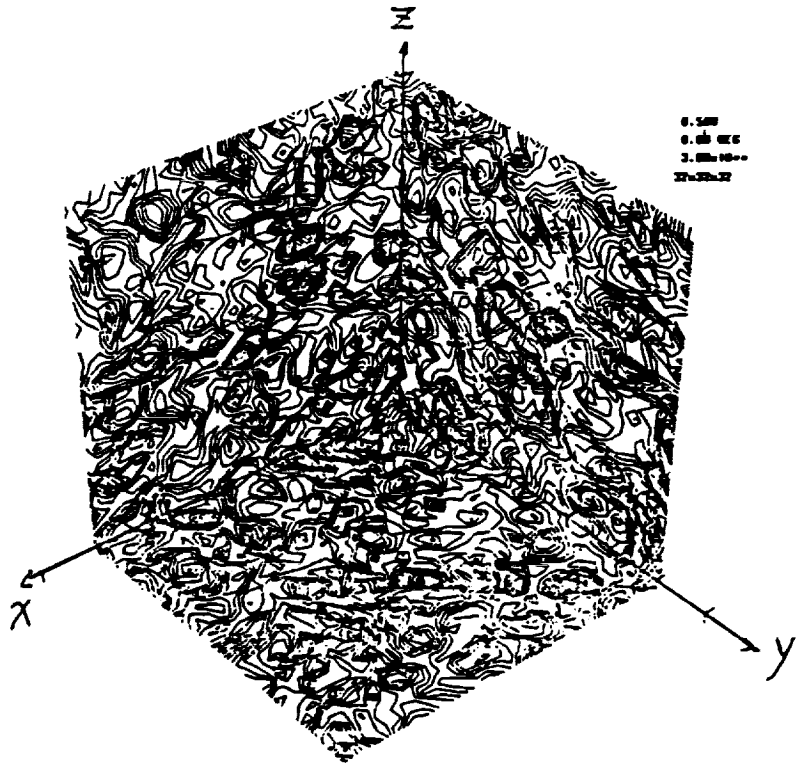

Figure 20. Flow structure without Coriolis Force, u-velocity.

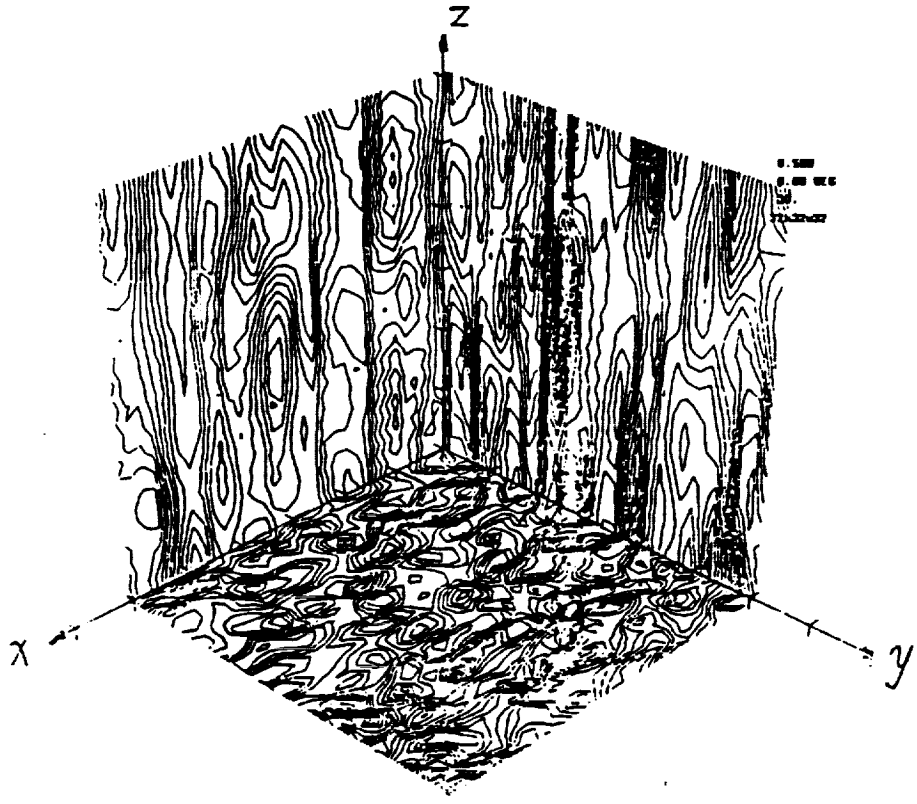

Figure 21. Flow structure with the Coriolis force, u-velocity.